Journal of The Electrochemical Society, 2021 **168** 070507

Evidence for Li^+/H^+ Exchange during Ambient Storage of Ni-Rich Cathode Active Materials

Louis Hartmann,[z] Daniel Pritzl, Hans Beyer, and Hubert A. Gasteiger[*]

Chair of Technical Electrochemistry, Department of Chemistry and Catalysis Research Center, Technical University of Munich, Munich, Germany

Layered Ni-rich transition metal oxides like so-called NCMs are one of the most-promising high-energy density cathode active materials (CAMs) for next-generation Li-Ion batteries. However, compared to NCMs with low nickel content, Ni-rich NCMs suffer from a highly reactive surface that leads to an accumulation of surface contaminants and also from a higher soluble base content. Since a detailed understanding of the formation rate of surface contaminants is still lacking, we will investigate the effect of extended storage in high relative humidity air of a Ni-rich NCM851005 ($Li_{1+\delta}(Ni_{0.85}Co_{0.10}Mn_{0.05})_{1-\delta}O_2$, with δ typically ~0.005–0.03) and a low nickel content NCM111 ($Li_{1+\delta}(Ni_{1/3}Co_{1/3}Mn_{1/3})_{1-\delta}O_2$) on the build-up of surface contaminants. The formation rate of the surface contaminants during this accelerated wet-storage test is quantified by TGA-MS under Ar. To elucidate the processes occurring during the TGA-MS experiments, as-received and wet-stored CAMs are introduced into an XPS chamber where they are heated in situ to different temperatures, followed by XPS analysis of the surface compositional changes. Comparative measurements with water-washed NCM851005 reveal the close analogy between the processes that occur during extended storage of NCMs in humid ambient air and during the washing of NCMs, commonly used to lower the soluble base content of Ni-rich NCMs.

 [DOI: 10.1149/1945-7111/ac0d3a]

Manuscript submitted May 10, 2021; revised manuscript received June 16, 2021. Published July 1, 2021. *This was paper 830 presented during PRiME 2020, October 4–9, 2020.*

2019 marks the year in which John B. Goodenough, M. Stanley Whittingham, and Akira Yoshino were awarded with the Chemistry Nobel Prize for their work on Li-Ion batteries. While this technology is already a viable option for stationary short-term energy storage and the electrification of the automotive sector, many challenges, such as cost, availability of transition metals, energy density, and charging time still need to be addressed.[1–5] Except for switching the cell chemistry completely to novel systems, such as the still not sufficiently mature Li-S and Li-O_2 batteries,[3,6–8] the most viable way to increase the energy density of Li-ion battery cells is to increase the capacity of the cathode active material (CAM). One approach to increase the performance and lower the cost of state-of-the-art layered transition metal oxide based NCM materials ($Li_{1+\delta}(Ni_xCo_yMn_z)_{1-\delta}O_2$, with $x + y + z = 1$ and δ typically ~0.005–0.03) is to increase their Ni content, whereby the cost can largely be reduced by minimizing the Co content[9–12] or by developing Co-free variants.[11,13,14] Cutting-edge materials with nickel contents corresponding to $x = 0.9$–0.95 are already being synthesized, and the research focus has been shifting towards pure $LiNiO_2$ (LNO).[15–18] The synthesis of highly Ni-rich NCMs and LNO is also rather challenging, illustrated in the case of LNOs by the observation that Ni^{2+} can easily diffuse onto the Li-sites and negatively affect the cycling performance of these materials.[16,19,20] This problem has been addressed by mild temperatures, high O_2-partial pressures, and the use of an over-stochiometric amount of lithium during calcination.[19,21–23]

While the low Ni content NCM111 ($x = y = z = 1/3$) has already been used for many years, its Ni-rich analogues ($x > 0.8$) suffer from thermal instability, rapid capacity fading, and a high sensitivity to the cycling and materials storage conditions.[24–27] The generally required lithium excess during synthesis of Ni-rich CAMs (see above) results in the formation of surface contaminants such as hydroxides and carbonates upon contact of Ni-rich CAMs with CO_2 and moisture.[28–30] These contaminants result in *chemical* reactions with the electrode and electrolyte components which result in an increase in cell gassing, gelation of the electrode coating slurries due to the presence of soluble bases, and diminished capacity retention.[25,31–35] The use of surface coatings, bulk dopants, and gas-treatments has been investigated to mitigate the gassing caused by surface contaminants or to remove surface contaminants and passivate the CAM surface.[36–40] A commonly employed mitigation strategy for commercially available CAMs consists of washing these materials with water, followed by a recalcination, which leads to a removal of the majority of the surface contaminants.[41,42] Washing also lowers the soluble base content, thereby improving the processability of the electrode coating slurry. However, washing with water does not only remove soluble bases, but evidence was found that it is also accompanied by an exchange of intercalated lithium ions with protons from the solution, resulting in a Li^+/H^+ exchange in the near-surface region of the CAM.[43] During mild heating (between ~250 °C–400 °C) of an H^+-containing NCM (or other lithium transition metal layered oxides), the formation of an O-depleted near-surface layer with a spinel-like structure is observed, concomitant with the release of water and oxygen.[43] This surface reconstruction and removal of surface contaminants (by reaction and/or desorption) results in a greatly reduces gassing of the washed materials.[44]

While there have been several studies examining the washing of Ni-rich cathode active materials or the effect of their exposure to humid ambient atmosphere, we here want to focus on the differences and similarities with regards to the fundamental processes that occur in the case of Ni-rich CAMs during both washing and exposure to humid ambient air. To study the latter, we applied an accelerated storage test, during which Ni-rich NCM851005 and, for comparison, low Ni content NCM111 are exposed to high relative humidity ambient air (referred to as wet-storage). After different storage times, ranging from 5 min to one week, the materials were characterized by TGA-MS with Ar as carrier gas and XPS. The processes occurring during heating of as-received, washed, and wet-stored materials were examined by an in situ XPS approach, where the CAM samples were heated up to 700 °C inside of the XPS main chamber, investigating the surface composition after different heating temperatures. Our studies reveal that the wet-storage of CAMs not only results in the formation of surface contaminants, but also in the exchange of intercalated lithium ions with protons, a process that is analogous to the Li^+/H^+ exchange in the near-surface CAM region that was proposed to occur during CAM washing, leading to the same O-loss mechanism during the re-calcination of both wet-stored and washed CAMs.

Experimental

Wet-storage and washing of CAMs.—The here used accelerated storage test, referred to as wet-storage, was described previously.[24]

*Electrochemical Society Fellow.
[z]E-mail: louis.hartmann@tum.de

Briefly, the two here studied polycrystalline NCM111 and NCM851005 CAMs (all BASF, Germany) have a BET surface area of around 0.3 $m^2\ g^{-1}$ (particle size: ~5–10 μm) and their morphology is similar to the NCM811 CAM characterized by Friedrich et al.[45] These were stored for up to one week in ambient air over an open water bath held at 25 °C, located in a vessel that contained a lid with a small hole to allow for intrusion of ambient air. This resulted in a controlled atmosphere with high relative humidity (measured RH of ~85 ± 5%) and a CO_2 concentration near the atmospheric concentration of ~400 ppm. For the washing process, purified Millipore water (15 MΩ cm, Merck KGaA, Germany) was used, whereby 5 g of NCM851005 were added into 25 ml of purified water and stirred with a magnetic stirrer for 20 min. Afterwards, the washed CAM was vacuum-filtrated.

All samples were dried in a glass oven (Büchi, Switzerland) for at least 4 h at 70 °C under dynamic vacuum to remove physisorbed H_2O, and subsequently stored in an Ar-filled glove box (<0.1 ppm O_2 and H_2O, MBraun, Germany) without exposure to ambient air after drying. A summary of the thus prepared samples is given in Table I.

X-ray photoelectron spectroscopy (XPS).—The surface analysis of the as-received, 1 week wet-stored, and washed NCM851005 was carried out by X-ray photoelectron spectroscopy (Axis, Supra, Kratos, UK). The powders were pressed into pellets inside an argon-filled glovebox and mounted on a heatable sample holder; from the glove box, the sample holder was quickly transferred through air into the XPS antechamber. The sample was kept in the antechamber until a pressure of ~10^{-8} Torr and was then transferred to the sample analysis chamber, where the pressure was always kept at ~10^{-9} Torr during the whole measurement period. Sample irradiation was carried out with monochromatic Al Kα radiation (1486.6 eV), using an emission current of 15 mA. Survey spectra were recorded for all samples with a stepsize of 0.5 eV and at a pass energy (PE) 160 eV. High-resolution spectra were recorded with a stepsize of 0.05 eV and a pass energy of 15 eV. For all measurements, the spectra were calibrated to the adventitious carbon peak with a binding energy (BE) of 284.8 eV. For the in-situ heating experiments, the filament and detector were turned off, while the sample holder was not moved during sample heating to the desired temperature at a rate of 0.1 K s^{-1}. The sample was kept at the desired temperature (250 °C, 350 °C, 450 °C, 700 °C, in sequence) for at least 3 h prior to recording XPS spectra at room temperature. The spectra were fitted using a mixture of a Lorentzian (30%) and Gaussian (70%) shape function on top of a Shirley background; the constraints on binding energy and full width at half maximum (FWHM) for the different species are given in Table II. The here assigned species will be discussed in more detail later. For the quantification of the O 1 s spectra in the relative intensities of the fitted peaks of oxygen-containing species were used. No relative sensitivity factor was needed as only different oxygen peaks were compared.

Thermogravimetric analysis with coupled mass spectrometry (TGA-MS).—For TGA-MS analysis, a TGA system (Mettler Toledo, Switzerland) coupled to a mass spectrometer (Pfeiffer Vacuum, Germany) was used. All analyzed samples were dried in a vacuum oven (Büchi, Switzerland) for at least 3 h at 70 °C under dynamic vacuum, placed into a Al_2O_3 crucible, and then transferred quickly into the TGA-MS, minimizing the exposure time to ambient air (the entire transfer required ~5 min, which was added to the time scale shown in Fig. 4, i.e., the as-received sample is depicted at a nominal storage time of 5 min). The as-received and wet-stored samples were analyzed with the following protocol: First a conditioning step at 25 °C for 10 min with an argon flow rate of 200 ml min^{-1} was done to remove any air left from the transfer. Afterwards, the flow rate was changed to the flowrate used during the experiment (20 ml min^{-1}) and another rest phase of 5 min at 25 °C was carried out. After these pre-treatment steps (not shown in the TGA-MS plots in this study), the temperature was increased from 25 °C to 120 °C at a rate of 10 K min^{-1}, followed by a temperature hold at 120 °C for 30 min. The last step includes a heat ramp (10 K min^{-1}) to 450 °C with a final hold phase of 30 min; an extended TGA-MS experiment was also performed with ramp to 1125 °C instead of 450 °C. Owing to the small mass losses in the range up to 450 °C, 100 mg of sample were used in the here shown TGA-MS experiments. All mass traces from the MS were normalized to the[36] Ar isotope signal (m/z = 36).

Results and Discussion

Characterization of wet-stored CAMs by TGA-MS and XPS.—To investigate the effect of ambient storage, we have chosen NCM851005, as its high Ni content makes it prone to surface contaminants, such as basic nickel carbonate ($NiCO_3{\cdot}2Ni(OH)_2{\cdot}xH_2O$, NiCBH), LiOH, and Li_2CO_3.[24,25,46] TGA-MS is used to quantify the overall amount of surface contaminants on the active materials as a function of storage time.

First, a TGA-MS experiment up to a high temperature of 1125 °C was done to determine the decomposition temperature of the Ni-rich

Table I. Cathode active materials used for TGA-MS and XPS analyses.

Sample designation	Base CAM	Treatment type	Treatment duration
as-received NCM851005	NCM851005	—	—
wet-stored NCM851005	NCM851005	storage at ~85% RH and ~400 ppm CO_2	1 h, 3 h, 10 h, 1 d, 4 d, 1 week
washed NCM851005	NCM851005	20 min wash with water (5:1 g:g H_2O:CAM)	20 min
as-received NCM111	NCM111	—	—
wet-stored NCM111	NCM111	storage at ~85% RH and ~400 ppm CO_2	1 h, 3 h, 10 h, 1 d, 4 d, 1 week

Table II. XPS peak fitting parameters used for identification and quantification of the different surface species of the as-received, wet-stored, and washed NCM851005 samples.

Element/region	Assigned species	Binding energy [eV] (constrained range)	FWHM [eV] (constrained range)
carbon C 1s	"adventitious carbon"	248.8 eV (fixed)	1.0–1.3
	"M-CO_3"	289.8 (±0.1)	1.0–1.3
oxygen O 1s	"layered oxide"	529.2 (±0.1)	1.0–1.3
	"O-depleted oxide"	530.0 (±0.1)	1.0–1.3
	"M-OH/CO_3"	531.3 (±0.2)	1.5–2.25
sodium Na KLL	Na KL_1L_{23}	533.3 (±0.2)	1.5–2.25

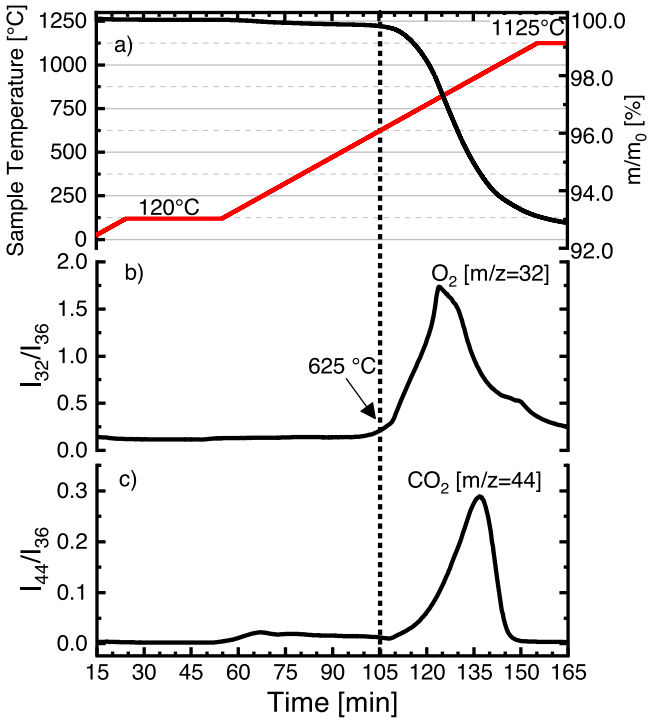

Figure 1. TGA-MS analysis of as-received (black lines) NCM851005 under Ar, with two temperature ramps at 10 K min^{-1} and temperature hold phases at 120 °C and 1125 °C. (a) Temperature profile (red line, left *y*-axis) and relative mass change of the sample (black line, right *y*-axis). MS traces normalized to the[36] Ar isotope for: (b) O_2 (m/z = 32) and (c) CO_2 (m/z = 44).

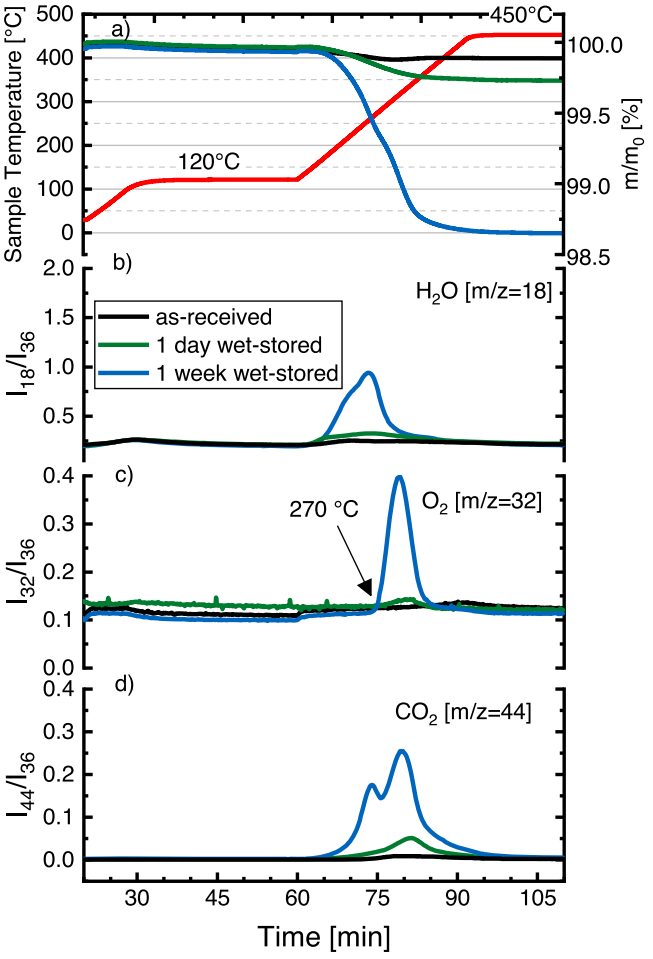

Figure 2. TGA-MS of as-received (black lines), 1 d wet-stored (green lines), and 1 week wet-stored (blue lines) NCM851005, conducted under Ar, with two temperature ramps at 10 K min^{-1} and temperature hold phases at 120 °C and 450 °C. (a) Temperature profile (red line, left *y*-axis) and relative mass changes of the different samples (right *y*-axis). MS traces normalized to the[36] Ar isotope for: (b) H_2O (m/z = 18), (c) O_2 (m/z = 32), and (d) CO_2 (m/z = 44).

NCM851005. Figure 1 shows the TGA-MS analysis of the as-received material, depicting the relative mass loss (Fig. 1a, black line and right *y*-axis) vs temperature (red line and left y-axis), as well as the corresponding mass traces of the evolved O_2 (Fig. 1b) and CO_2 (Fig. 1c) normalized to the[36] Ar isotope signal.

For the Ni-rich NCM851005, a significant mass loss initiates at ∼625 °C, resulting in an overall loss of ∼6.7% by the time the maximum temperature of 1125 °C is reached. This mass loss is accompanied by sharp oxygen (Fig. 1b) and CO_2 (Fig. 1c) evolution features. The onset temperature for the observed O_2 evolution is consistent with the literature values for the bulk oxygen loss from fully lithiated Ni-rich NCMs.[24] By comparing this data with references from our earlier studies, we conclude that the CO_2 evolution at temperatures over ∼625 °C stems from the decomposition of a Li_2CO_3 surface contaminant phase.[24,47] It originates either from residual Li_2CO_3 from the CAM synthesis (either done with Li_2CO_3 or with battery-grade LiOH that commonly has a ∼1% Li_2CO_3 content[48]) or from unintentional exposure to humid ambient air and the accompanied reaction of H_2O and CO_2 on the CAM particle surface to form Li_2CO_3.[49] As both processes—bulk oxygen release and Li_2CO_3 decomposition—overlap, a quantification of the amount of Li_2CO_3 contaminants of the CAM via TGA-MS is unfortunately not possible for NCMs. In addition to these features at high temperature, more subtle changes are also noticeable at lower temperatures. A small mass loss is visible between 120 °C and 625 °C, which is accompanied by a small CO_2 evolution feature with a maximum at ∼250 °C (after ∼70 min in Fig. 1). No oxygen release is seen below ∼625 °C.

Therefore, our focus will be shifted to the temperature range of 25 °C to 450 °C. This allows for a shorter measurement time and the characterization of all other surface contaminants, except for Li_2CO_3 and Li_2O which only decompose at temperatures beyond 700 °C (note that Li_2O surface contaminants would readily react to LiOH and then to Li_2CO_3 when exposed to ambient humid air, so that Li_2O is not expected to be present after wet-storage).[47] To understand the formation rate of surface contaminants on NCM851005, it was stored between 5 min and 1 week in high-RH air (∼85% RH), representing an accelerated storage test. Figure 2 depicts the TGA-MS analysis of as-received NCM851005 (black line) stored in a glovebox (<0.1 ppm O_2 and H_2O), as well as the same NCM851005 that was stored for 1 d (1 d wet-stored, green line) or for 1 week (1 week wet-stored, blue line) under the wet-storage conditions outlined in the Experimental section. The lower panels of Fig. 2 show the corresponding[36] Ar signal normalized mass traces of H_2O (Fig. 2b), O_2 (Fig. 2c), and CO_2 (Fig. 2d).

Towards the end of the first temperature ramp from 25 °C–120 °C, a minor mass loss is seen for every sample, extending somewhat into the first temperature hold phase at 120 °C (Fig. 2a). This mass loss is accompanied by a small and broad MS signal for H_2O (Fig. 2b), which is consistent with the removal of adsorbed water from the NCM851005 sample and the porous alumina crucible; as this signal was also visible for a blank measurement without CAM sample, it is not relevant for the following further discussion on CAM surface contaminants.

The mass loss at higher temperatures (>120 °C), however, deviates between the different NCM851005 samples. While the as-received CAM only has a mass loss of ∼0.1%, between 120 °C and 450 °C (black line in Fig. 2a), the wet-stored CAMs have a mass loss of ∼0.3% and ∼1.3% for the 1 d wet-stored (green line) and the

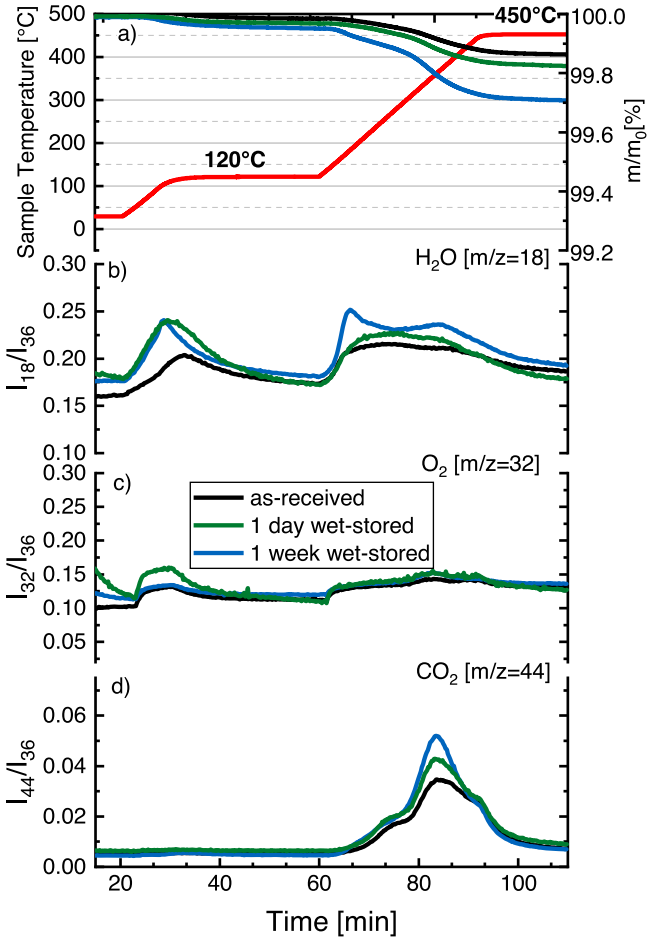

Figure 3. TGA-MS of as-received (black lines), 1 d wet-stored (green lines), and 1 week wet-stored (blue lines) NCM111, conducted under Ar, with two temperature ramps at 10 K min^{-1} and temperature hold phases at 120 °C and 450 °C. (a) Temperature profile (red line, left *y*-axis) and relative mass changes of the different samples (right *y*-axis). MS traces normalized to the[36] Ar isotope for: (b) H_2O (m/z = 18), (c) O_2 (m/z = 32), and (d) CO_2 (m/z = 44).

1 week wet-stored (blue line) CAM, respectively. Thus, more and more surface contaminants form on the CAM particles during prolonged wet-storage times, which decompose upon heating of the sample to 450 °C. A similar trend can be seen for the MS traces for H_2O (Fig. 2b), O_2 (Fig. 2c), and CO_2 (Fig. 2d), with the amount of evolved gas being the highest for the 1 week wet-stored NCM851005. The onset of H_2O evolution occurs at ∼160 °C for every sample (albeit very little for the as-received NCM851005), which can be attributed to the decomposition of surface hydroxides.[24,25] The onset of CO_2 evolution is observed at roughly the same temperature for the wet-stored CAMs and at a somewhat higher temperature for the as-received CAM, whereby the CO_2 signal peak height increases ∼6-fold between the as-received and the 1 d wet-stored CAM and by another factor of ∼5 between the latter and the 1 week wet-stored CAM. Both the H_2O and CO_2 evolution seen for the wet-stored CAMs closely match the characteristic decomposition of $NiCO_3{\cdot}2Ni(OH)_2{\cdot}xH_2O$ that occurs at significantly lower temperatures than $MnCO_3{\cdot}xH_2O$ and $CoCO_3{\cdot}xH_2O$ that were shown to decompose above 220 °C.[24] This is also reasonable, as the molar concentration of Ni is also much higher than those of Mn and Co, so that even for equal reactivity with H_2O and CO_2, the Ni based contaminant would be dominant. While the splitting of the CO_2 feature is reproducible, we currently do not have an explanation for it.

As was already observed in Fig. 1, the as-received NCM851005 does not exhibit any O_2 release at temperatures below ∼625 °C, consistent with the data in Fig. 2c. Surprisingly, however, oxygen evolution at much lower temperatures is seen for the wet-stored samples, with an onset temperature of ∼270 °C (Fig. 2c). While the O_2 peak in this low temperature region is rather small for the 1 d wet-stored sample (green line), it increases dramatically for the 1 week wet-stored sample. These here described gas evolution features in the low temperature region were also seen in earlier studies for washed NCM851005 CAMs, and this similarity between washed and wet-stored CAMs will be critically compared later on.

Compared to the significant mass losses particularly for the wet-stored NCM851005 samples, Fig. 3 shows that they are ∼1.5 and ∼4 times lower for the 1 d and 1 week wet-stored NCM111, respectively. While the evolution of H_2O towards the end of the first temperature ramp from 25 °C–120 °C (see Fig. 3b) is of the same magnitude as in the case of NCM851005, the second H_2O evolution onset at ∼160 °C is substantially smaller; at the same time, the O_2 evolution signal is within the baseline noise even for the wet-stored NCM111 (see Fig. 3c). The differences in the signal magnitude for the evolution of CO_2 ascribed to the decomposition of basic transition metal carbonates closely follow the above-described differences in mass loss. In summary, the sensitivity towards the accumulation of surface contaminants is substantially less for low Ni content NCMs compared to Ni-rich NCMs, consistent with previous findings.[24,25,49]

Build-up of surface contaminants with time of wet-storage.—To correlate the increase of surface contaminants over storage time, the TGA-MS derived mass loss between 120 °C to 450 °C for NCM851005 (orange dots) as-received and for NCM851005 wet-stored for 1 h, 3 h, 10 h, 1 d, 4 d and 1 week were plotted against their respective storage times. To the effect of Ni content on the accumulation of surface contaminants, the Ni-rich NCM851005 was compared with a low Ni content NCM111 CAM (black dots; the same material as that used in an earlier study[24]), which is considered to be more stable in ambient air.[24,25] The mass loss data vs storage time are depicted in Fig. 4; here, the 5 min required to load the samples into the TGA-MS instrument during which the samples were exposed to ambient air were added to the wet-storage time, so that the as-received CAMs are plotted at an *x*-axis value of 5 min. It should be noted that both CAMs were stored together in the same vessel in order to eliminate the effect of possible minor changes in the storage conditions.

Figure 4 shows that both CAMs exhibit an increase in mass loss with wet-storage time. The TGA-MS derived mass loss for the as-received CAMs (left-most points in Fig. 4) is higher for NCM851005 (∼0.11%) compared to NCM111 (∼0.02%), suggesting a higher amount of surface contaminants on the Ni-rich NCM, as found in earlier measurements.[24] Furthermore, the absolute increase in mass loss after 1 d of wet-storage (5th data points from the left, at 1440 min) at ∼85% RH in ambient air (∼400 ppm CO_2) and 25 °C is again higher for NCM851005 (by ∼0.18% to ∼0.28%) compared to NCM111 (by ∼0.10% to ∼0.12%). This faster increase of the mass loss for the Ni-rich NCM becomes even more pronounced after 1 week of wet-storage (right-most data points, at 10080 min), where the total mass loss amounts to ∼1.25% for NCM851005 compared to only ∼0.18% for NCM111. Overall, these data confirm the higher susceptibility of Ni-rich NCMs for the accumulation of surface contaminants upon exposure to humid air compared to low Ni content NCMs.[24,49,50]

XPS analysis of wet-stored and wet-stored + heat-treated NCM851005.—The characterization of the wet-stored material by TGA-MS already brought some insight into the formation of surface contaminants, suggesting on the basis of the observed decomposition temperature that basic nickel carbonate constitutes a significant fraction of the surface contaminants on Ni-rich NCMs. Further mechanistic insights can be obtained by XPS measurements, particularly through monitoring the surface processes that occur

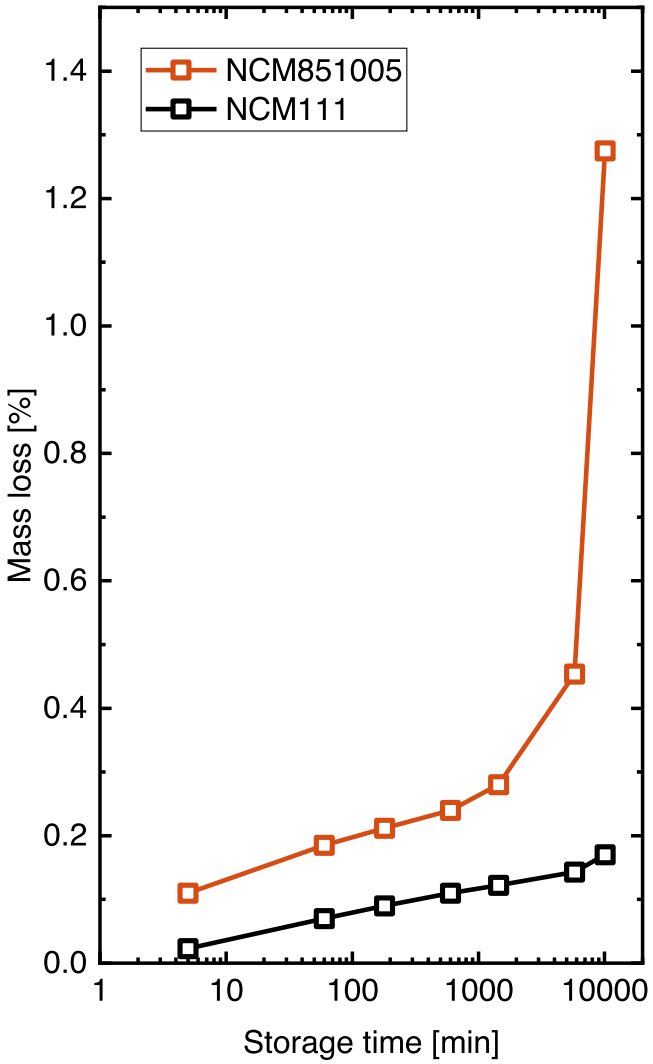

Figure 4. Relative mass-loss obtained from TGA-MS measurement between 120 °C and 450 °C of NCM851005 (in orange) and NCM111 (in black) for either the as-received CAMs (left-most data points) or for the CAMs after different times of wet-storage in high-RH (∼85%) ambient air at 25 °C. Both CAM types were stored simultaneously (up to 1 week or 10080 min) in the same storage vessel to minimize differences in storage conditions.

during the heating of wet-stored NCM851005, providing further insights into the gas release mechanism observed during the TGA-MS measurements under Ar. For this, as-received and 1 week wet-stored NCM851005 samples were mounted on a heatable sample holder and introduced into the XPS chamber, acquiring XPS data prior to any heating as well as after heating in the XPS chamber to different temperatures. The spectra in the O 1 s region were fitted with peaks assigned to the layered oxide phase, to an O-depleted oxide phase (representing spinel or rocksalt phases), and to one peak representing the oxygen signal from hydroxide and carbonate surface contaminants; the latter species strongly overlap, so that only one broad peak assigned to both species can be fitted in a meaningful manner. As will be apparent when discussing the spectra for the heat-treated samples, the NCM851005 CAM does contain small amounts of sodium (likely Na_2SO_4, stemming from the synthesis process[51]) that apparently segregates to the surface during heating, as was also observed in studies with Li- and Mn-rich NCM.[52,53] Therefore, the relatively strong sodium KL_1L_{23} Auger peak that appears at a binding energy value of ∼533 eV when using an Al Kα source also had to be included when fitting the peaks in the O 1 s region of the spectrum. That it is indeed sodium that is responsible for the strong signal at ∼533 eV in the spectra of the heat-treated samples is evident by the clear Na 1 s and Na $KL_{23}L_{23}$ features that are visible in the survey spectra of heat-treated samples (see Fig. A·1 in the Appendix). Both literature values[45,54–58] and references measured in-house were used to set the ranges and constraints for the binding energy and the FWHM values for the various fitted species (listed in Table II).

Figure 5 depicts the O 1 s region of NCM851005 as-received (panel a) and after 1 week wet-storage (panel b), marking the peak fits for the layered oxide with a peak at 529.2 ± 0.1 eV (green) and the peak representing surface hydroxides/carbonates at 531.3 ± 0.2 eV (blue, labeled M-OH/CO_3); no significant peak fits were obtained for the sodium Auger signal and for the O-depleted phase for these samples. The relative amounts of the peak integrals of the oxygen-containing peaks are quantified in Fig. 6. The as-received NCM851005 already has a high amount of hydroxide/carbonate surface contaminants, as seen by the most pronounced peak at 531.5 eV, and also a smaller peak at 529.1 eV, representing the bulk layered oxide (Fig. 5a). The peak height and area of the hydroxide/carbonate surface contaminants relative to the that of the layered oxide feature increases significantly for the 1 week wet-stored NCM851005 (Fig. 5b). As seen in Fig. 5 (two left-most data points), the ratio of M-OH/CO_3 to the layered oxide increases from ∼3/1 (≡76%/26%) for the as-received CAM to ∼7/1 (≡86%/12%) for the 1 week wet-stored CAM. This can be explained by an accumulation of hydroxide/carbonate surface contaminants during wet-storage, shielding the signal from the underlying lattice oxygen in the layered structure. As a rough estimate, a lowering of the layered oxide signal by ∼2.2-fold would imply an increase of the hydroxide/carbonate film thickness of on the order of λ·ln(2.2), where λ is the mean free path at a kinetic energy of ∼1 keV (i.e., in the O 1 s region for an Al Kα source) which is ∼3 nm, equating to an increase in the hydroxide/carbonate film thickness by ∼2.3 nm.[59]

By heating the 1 week wet-stored NCM851005 to 250 °C in the XPS chamber for 3 h (Fig. 5c), the ratio of hydroxide/carbonate surface contaminants (blue) to lattice oxygen (green) is drastically changed. The peak assigned to the layered oxide (green) is now more intense, suggesting a decomposition of surface contaminants, as is expected based on the onset of H_2O and CO_2 evolution at ∼160 °C observed in the TGA-MS experiment (see Fig. 2) and based on the fact that previous TGA-MS experiments showed that $NiCO_3{\cdot}2Ni(OH)_2{\cdot}xH_2O$ starts to decompose at ∼180 °C and is completely decomposed at ∼350 °C.[24] Furthermore, a fitting of the O 1 s region now requires the addition of an O–depleted oxide phase at 530.0 ± 0.1 eV (orange line) due to the loss of oxygen that in the TGA-MS experiments initiated at ∼270 °C, i.e., very close to the 250 °C temperature hold over 3 h in this experiment. Based on the peak fitting of the data in Fig. 5c, the relative fraction of the signals from the layered oxide (∼15%) and the O-depleted oxide (∼8%) shown in Fig. 6 now equates to ratio of M–OH/CO_3 to the layered plus O–depleted oxide of ∼3/1 (≡77%/(15% + 8%)), which is similar to that of the as-received NCM851005, consistent with the above hypothesized significant decomposition at 250 °C of surface contaminants that had formed during wet-storage.

Upon further heating this sample to 350 °C in the XPS chamber (Fig. 5d), the lattice oxygen features change drastically, with now a pronounced O-depleted oxide peak at ∼530.0 eV (orange) and only minor contributions from the layered oxide (green), suggesting the formation of a reasonably thick O-depleted near-surface layer. This is consistent with the nearly completed O_2 release at 350 °C observed in the TGA-MS experiment for the 1 week wet-stored sample (Fig. 2). Interestingly, this oxygen evolution is also known for washed NCM851005.[43] At the same time, the peak assigned to surface contaminants at 531.5 eV (blue) is still dominating the spectrum, even though $NiCO_3{\cdot}2Ni(OH)_2{\cdot}xH_2O$ should be completely decomposed at this temperature.[24] This is due to the fact that LiOH and Li_2CO_3 surface contaminants do not decompose below ∼450 °C and ∼700 °C, respectively.[47] Overall, however, the relative

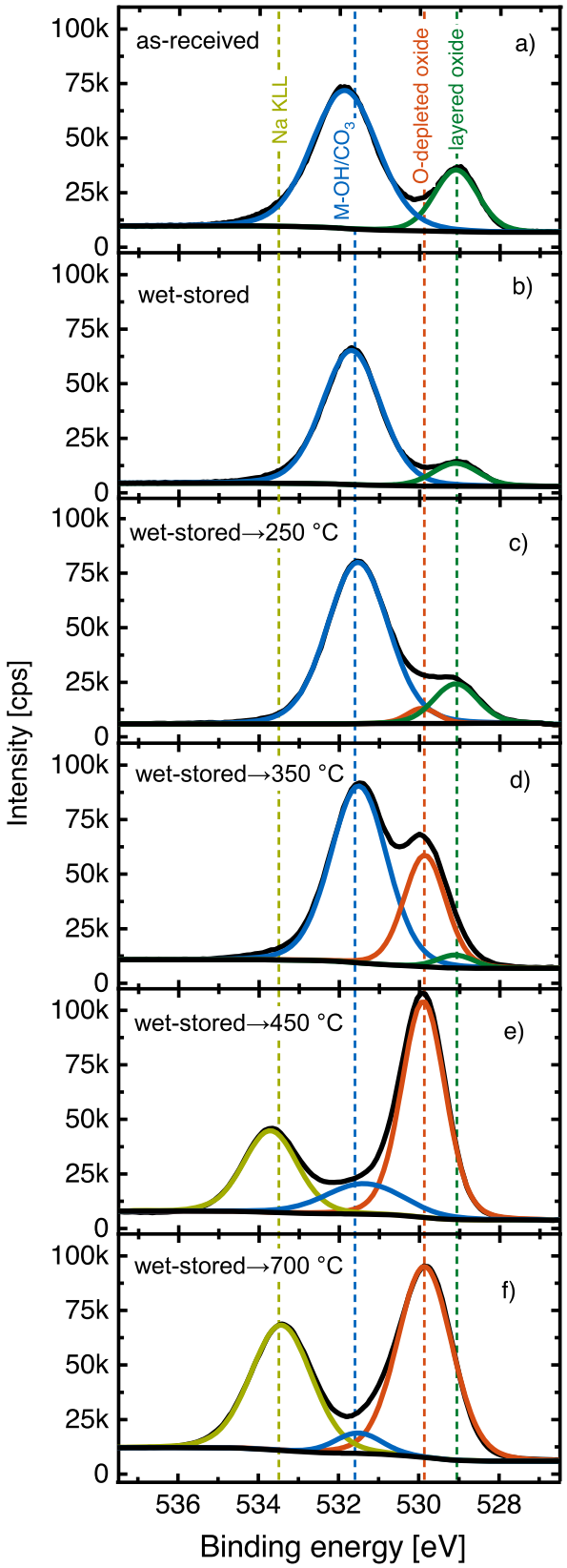

Figure 5. XPS data of the O 1 s region of NCM851005 samples: (a) as-received, and, (b) after 1 week of wet-storage. Furthermore, the 1 week wet-stored NCM851005 was heated inside of the main XPS chamber to the following temperatures and held there for 3 h prior to recording XPS data at room temperature: (c) 250 °C; (d) 350 °C; (e) 450 °C; and, (f) 700 °C. All samples were dried at 70 °C prior to the measurement and transferred to the XPS chamber with minimized air exposure.

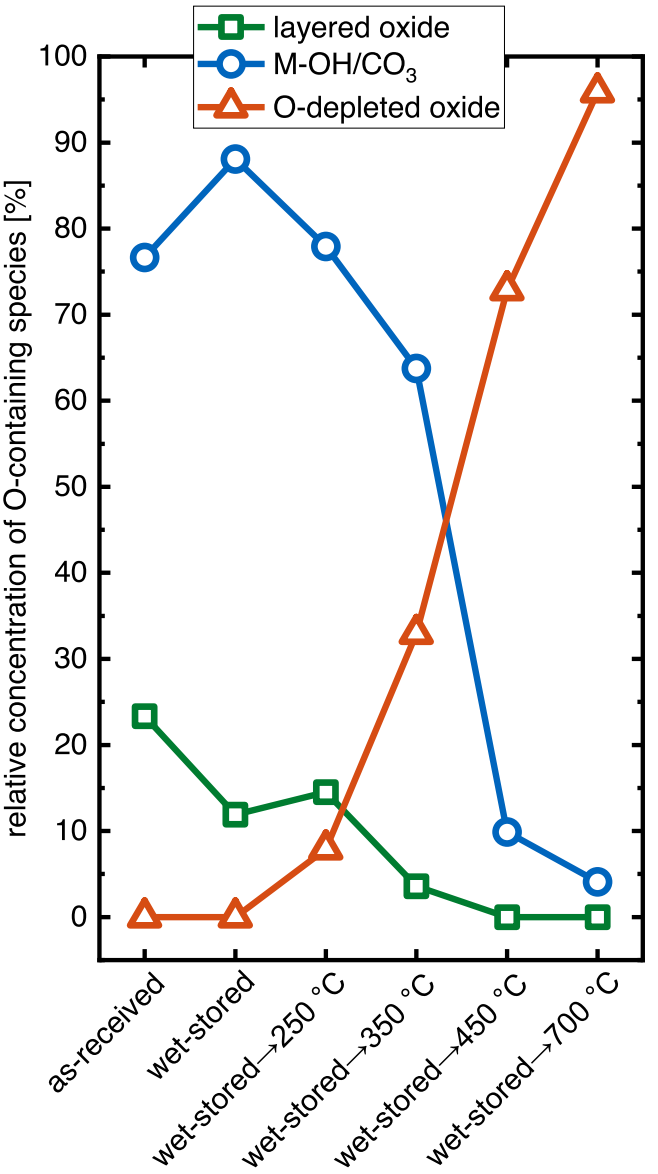

Figure 6. Quantification of the surface concentration of oxygen containing species for the spectra shown in Fig. 5.

fraction of the signals from the layered oxide (∼4%) and the O-depleted oxide (∼32%) shown in Fig. 6 now equates to a ratio of M-OH/CO_3 to the layered plus O–depleted oxide of ∼2/1 (≡64%/(4% + 32%)), marking a clear decrease in the amount of surface contaminants.

Further heating of the 1 week wet-stored sample to 450 °C (Fig. 5e) leads to a clear reduction of the hydroxide/carbonate feature, which can be explained by the decomposition of LiOH at this temperature.[47] No more features from the layered oxide can be discerned, indicating a further growth of the O-depleted surface layer. At the same time, a pronounced sodium Auger peak has appeared (yellow), which we ascribe to the temperature-driven surface segregation of sodium (note that no significant peak fits were obtained for the sodium Auger signal in the samples heated to 250 °C and 350 °C). The fact that this is also accompanied by the appearance of sulfur (see orange line in Fig. A·1 in the Appendix) suggests that the sodium signal is due to the surface segregation of Na_2SO_4. Finally, after heating to 700 °C, the hydroxide/carbonate feature has essentially vanished, consistent with the decomposition of Li_2CO_3 at ∼700 °C, while the feature for sodium has still increased somewhat.

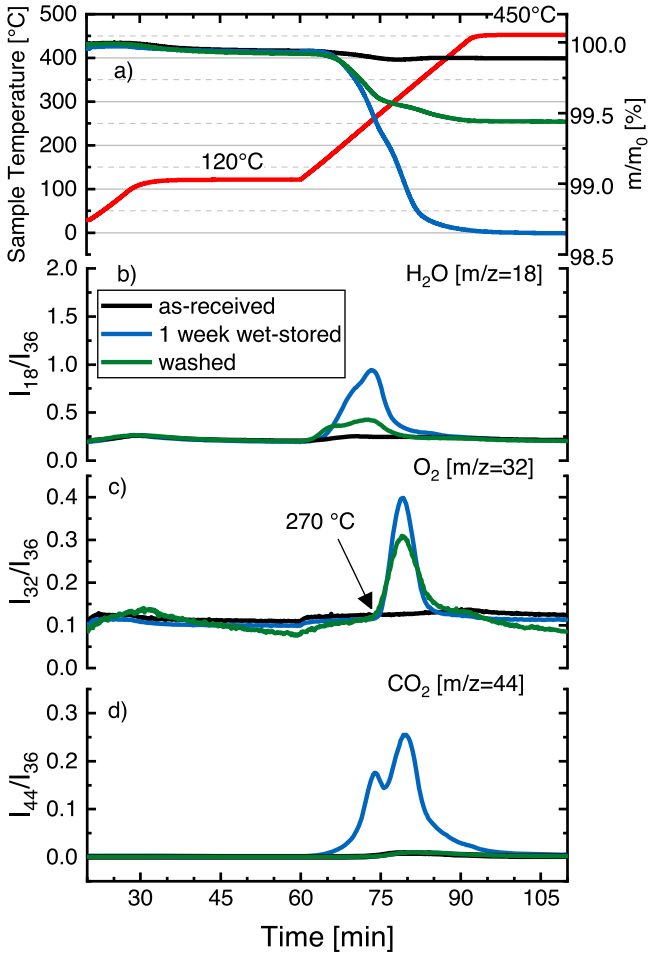

Figure 7. TGA-MS of as-received (black lines), 1 week wet-stored (blue lines), and washed (green lines) NCM851005, conducted under Ar, with two temperature ramps at 10 K min^{-1} and temperature hold phases at 120 °C and 450 °C. (a) Temperature profile (red line, left *y*-axis) and relative mass changes of the different samples (right *y*-axis). MS traces normalized to the[36] Ar isotope for: (b) H_2O (m/z = 18), (c) O_2 (m/z = 32), and (d) CO_2 (m/z = 44).

Comparison of wet-stored and washed NCM851005.—To better understand the similarities of wet-storage and washing of active materials, NCM851005 CAMs were analysed after 1 week of wet-storage and after a strong washing procedure (20 min at a 5:1 g:g H_2O:CAM ratio, as used previously[43]). Figure 7 depicts the TGA-MS experiments with as-received NCM851005 (black lines) that was stored in a glovebox (<0.1 ppm O_2 and H_2O), as well as with NCM851005 samples after 1 week wet-storage (blue lines) or after washing (green lines). The TGA-MS results for the first two samples were already discussed earlier (see Fig. 2), whereby little mass loss and gas evolution are observed for the as-received NCM851005, while the 1 week wet-stored NCM851005 displays a substantial mass loss, accompanied by the onset of H_2O and CO_2 evolution at ~160 °C due to the decomposition of surface contaminants (believed to be mostly $NiCO_3{\cdot}2Ni(OH)_2{\cdot}xH_2O$) as well as by O_2 evolution at ~270 °C (blue lines in Fig. 7).

Quite strikingly, the mass loss profile and the H_2O and O_2 evolution profiles are essentially identical between the washed and the wet-stored NCM851005, despite of the overall lower magnitude of the mass loss (~2.5-fold) and of the H_2O (~3-fold) and O_2 (~1.5-fold) signals for the washed NCM851005. In our previous study by Pritzl et al.[43] on the processes that occur during the washing and subsequent heating of NCM851005, pH measurements indicated the occurrence of a Li^+/H^+ exchange in the near-surface region of the CAM particle during the washing step:

$$Li^+|_{NCM} + H_2O \rightarrow H^+|_{NCM} + Li^+ + OH^- \quad [1]$$

Upon heating of washed NCM851005, the protonated near-surface region (simplistically referred to as MOOH) was proposed to first decompose into a spinel-like phase with a predominant loss of H_2O according to Eq. 2 (the signal near ~160 °C in Fig. 7b):

$$MOOH \rightarrow \frac{1}{3}M_3O_4 + \frac{1}{2}H_2O + \frac{1}{12}O_2 \quad [2]$$

At higher temperature, this process is, followed by the conversion to a rocksalt-like phase concomitant with the evolution of O_2 according to Eq. 3 (the signal near ~270 °C in Fig. 7c):

$$M_3O_4 \rightarrow 3\,MO + \frac{1}{2}\,O_2 \quad [3]$$

In view of the essentially identical profiles for the mass loss and the evolution of H_2O and O_2 for the 1 week wet-stored and the washed NCM851005 samples, we hypothesize that both treatments, namely exposure to humid ambient air and washing of particularly Ni-rich NCMs are accompanied by a Li^+/H^+ exchange in the near-surface region of the CAM particle.

The striking difference, however, between the 1 week wet-stored and the washed NCM851005 is the lack of any CO_2 evolution of the latter (green line in Fig. 7d). In the case of the wet-stored sample, the CO_2 and part of the H_2O evolution were ascribed to the decomposition of transition metal carbonates (believed to be mostly $NiCO_3{\cdot}2Ni(OH)_2{\cdot}xH_2O$ for Ni-rich NCMs), which would also be expected to form during the here conducted washing of NCM851005 under ambient air atmosphere, i.e., in the presence of dissolved CO_2. However, as shown by titration experiments in a previous publication, washed materials do not any more contain soluble carbonates on their surface,[43] so that the missing CO_2 evolution in the TGA-MS measurement can be explained by the dissolution of carbonates in the washing solution and their subsequent removal during filtration. This is further supported by the C 1 s spectra of the washed NCM851005, which in contrast to the as-received and the 1 week wet-stored sample does not show a significant signal in the typical binding energy range known for carbonates (~290 eV), as shown in Fig. 8. The (partial) removal of basic hydrated carbonates during washing also explains the lower H_2O evolution of the washed compared to the wet-stored material in the TGA-MS experiments (Fig. 7b). Note: basic nickel carbonate with a solubility of 0.093 g l^{-1} for NiCBH, roughly 0.05% wt can be dissolved for the here used washing parameters.

In summary, the TGA-MS analysis strongly suggests that a Li^+/H^+ exchange occurs during wet-storage of particularly Ni-rich NCMs, analogous to what was found when washing these materials. This hypothesis will be evaluated by further XPS measurements, examining the effect of a heat-treatment at 450 °C in the XPS chamber of as-received, 1 week wet-stored, and washed NCM851005. This is shown in Fig. 9, whereby the spectra for the as-received (a), the wet-stored (c), and the wet-stored + heated (d) NCM851005 are identical with those shown in Figs. 5a, 5b, and 5e, respectively; for a detailed discussion of these spectra please refer to that earlier section.

Analogous to the observations when heating the wet-stored NCM851005 to 450 °C (Fig. 9d), heating of the as-received CAM (Fig. 9b) results in the appearance of a strong sodium Auger peak (likely due to surface segregation of Na_2SO_4) and in a drastic lowering of the amount of hydroxide/carbonate surface contaminants. A small amount of the M-OH/CO_3 feature can still be fitted to the spectra, which we believe stems from remaining Li_2CO_3 contaminant that only decomposes at temperatures above ~625 °C (see Fig. 1). The striking difference between these 450 °C heated NCM851005 samples, however, is that the signals from the oxide phase in the case of the heated wet-stored NCM851005 correspond exclusively to that of an O-depleted oxide (orange, Fig. 9d), while that of the heated as-received NCM851005 has a very pronounced

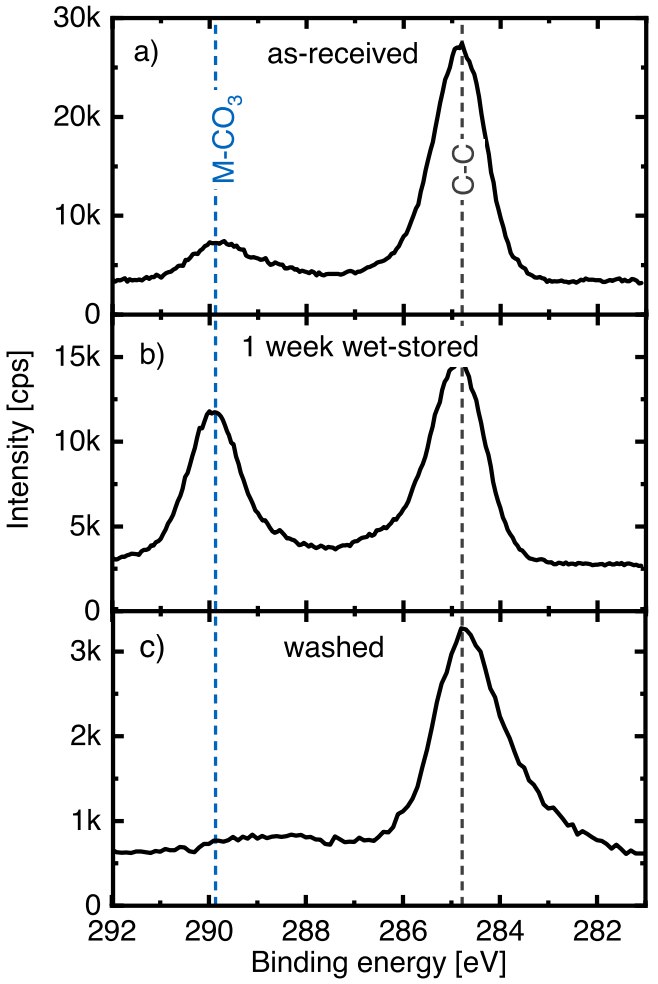

Figure 8. XPS data of the C 1 s region of NCM851005 samples: (a) as-received, (b) 1 week wet-stored, and (c) washed (5:1 g:g H_2O/CAM for 20 min at 25 °C). The adventitious carbon peak (C–C) fixed to 248.8 eV and the carbonate peak (M-CO_3) with a peak at 289.8 ± 0.1 eV are marked by the dashed vertical lines.

layered oxide peak (green, Fig. 9b), with only a rather small peak that can be fitted to the O-depleted oxide phase. Based on the above outlined hypothesis that the formation of an O-depleted oxide phase in the near-surface region of NCMs at temperatures below ∼625 °C requires a prior Li^+/H^+ exchange as described by Eqs. 1–3 (or, alternatively, partial (electro)chemical delithiation),[27,43,60,61] no such phase should indeed be observed for the 450 °C heated NCM851005; the minor amount of an O-depleted oxide phase deduced from the peak fitting suggests that the CAM must have been exposed to humidity during packaging and/or handling.

The spectrum of a washed unheated material (Fig. 9e) is qualitatively similar to that of the as-received CAM, which is surprising, as one would have expected the absence of the hydroxide/carbonate feature (blue) due to the removal of soluble hydroxide/carbonate surface contaminants during washing, evidenced by the spectrum in the C 1 s region that clearly shows the absence of carbonates (see Fig. 8c). The only explanation for this is that residual water remaining in the pores of the material after the removal of the washing solution by filtration facilitates a continued Li^+/H^+ exchange (according to Eq. 1), leading to the re-formation of LiOH (and perhaps other transition metal hydroxides) that is represented by the observed M-OH/CO_3 feature. After heating the washed NCM851005 at 450 °C (Fig. 9f) a clear formation of the O-depleted oxide phase is marked by the peak at ∼530.0 eV in the XPS spectrum, identical with what was observed for the 450 °C heated wet-stored NCM851005 (Fig. 9d). Thus, heating both washed and wet-stored Ni-rich NCMs to 450 °C in an oxygen-free environment (i.e., in a TGA under Ar or in vacuum) results in the formation of an O-depleted oxide phase in the near-surface region of the NCM particles, representing spinel-like or rocksalt-like phases. Therefore, wet-stored and washed materials experience a similar surface reconstruction upon heating, facilitated by the Li^+/H^+ exchange during wet-storage and washing.

Last, it should be noted that the washed and 450 °C heated NCM851005 has a significantly smaller amount of sodium on its surface (yellow, Fig. 9f) that the as-received and 450 °C heated NCM851005 (Fig. 9d). This can be understood by considering that the washing of polycrystalline NCMs results in a ∼4-fold increase in specific surface area due to crack formation between the primary crystallites.[45,58] Thus, as most sodium salts are highly soluble in water, sodium-based contaminants in the outer surface region of polycrystalline NCMs are likely removed by washing, so that the sodium surface segregation during heating is reduced.

In summary, storage under humid ambient conditions of NCMs leads not only to the formation of surface contaminants by the reaction of the transition metals with H_2O and atmospheric CO_2, such as the basic nickel carbonate, but analogous to the washing of NCMs, a Li^+/H^+ exchange in the near-surface region of the NCM particles occurs, concomitant with a release of LiOH. A subsequent

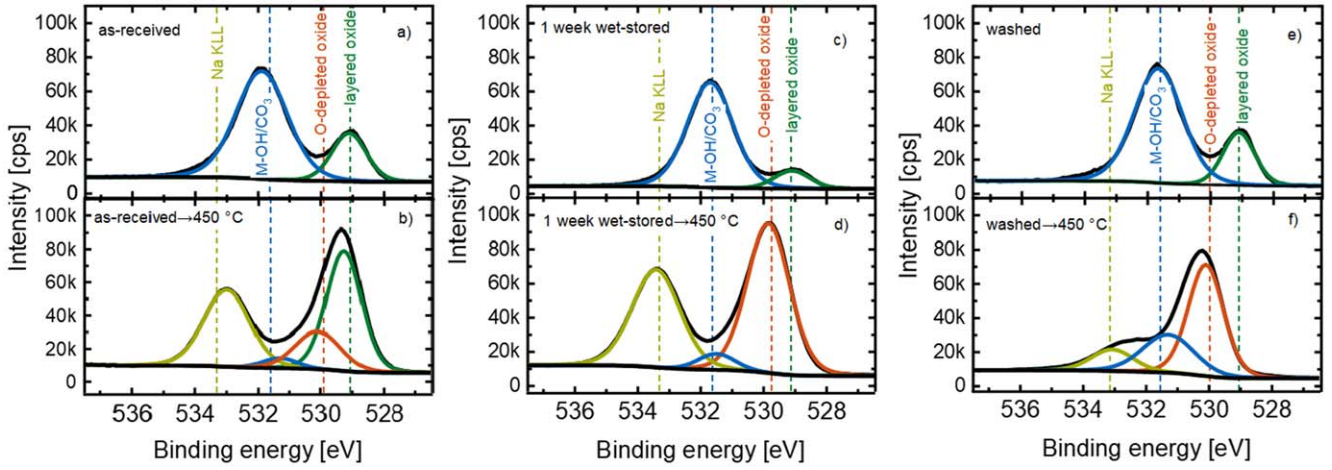

Figure 9. XPS data of the O 1s region of NCM851005 samples: (a) as-received, (c) 1 week wet-stored, and (e) washed (5:1 g:g H_2O/CAM for 20 min at 25 °C). These NCM851005 samples were subsequently heated to 450 °C in the XPS chamber and analyzed by XPS (b), (d), and (f). All samples were dried at 70 °C prior to the measurement and transferred to the XPS chamber with minimized air exposure.

heat-treatment at 250 °C or higher of washed or wet-stored Ni-rich NCM851005 was shown to lead to the formation of an O-depleted oxide phase in the near-surface region of the NCM particles, triggered by the reaction of exchanged H^+ and accompanied by the release of H_2O and O_2. Based on a comparison of the TGA-MS experiments with wet-stored NCM851005 (Fig. 2) and NCM111 (Fig. 3), the much reduced release of H_2O and O_2 in case of the latter suggests its much reduced reactivity towards the Li^+/H^+ exchange reaction.

Conclusions

In this study, we have applied an accelerated the wet-storage procedure to examine the processes that occur during the exposure of Ni-rich cathode active materials (CAMs) to humid ambient air, which is known to compromise their battery performance. In particular, we used TGA-MS to investigate the formation-rate of the surface contaminants during the wet-storage of NCM851005, comparing it with the low Ni content NCM111 CAM. In order to gain further insights into the processes observed during the TGA-MS experiments conducted with Ar, the as-received NCM851005 as well as the wet-stored NCM851005 before and after heat-treatment in the XPS chamber under vacuum were analyzed by XPS.

The mass loss between 120 °C–450 °C during TGA-MS experiments of as-received and wet-stored NCMs was shown to correlate with the formation of surface contaminants, showing that their relative amount increases with time of wet-storage and with Ni content of the NCMs. The observed mass loss was accompanied by the onset of H_2O evolution at ∼160 °C and of O_2 at ∼270 °C. XPS measurements of wet-stored NCM851005 heated at different temperatures in the XPS chamber revealed the formation of an O-depleted surface layer upon heating at 250 °C, becoming very pronounced at 350 °C and beyond.

Analogous experiments with NCM851005 washed in water showed the same gas evolution profiles in the TGA-MS experiments and the same compositional evolution with temperature in XPS measurements. This provides strong evidence that the same processes occur during wet-storage and washing, namely a Li^+/H^+ exchange in the near-surface region of the NCM particles that results in the formation of an oxygen-depleted spinel-like surface phase upon heating to ∼160 °C and a rocksalt-like surface layer upon heating to ∼250 °C. Different to wet-stored NCM851005, the washed material did not contain any surface carbonates any more, but still contained surface hydroxides, which we believe derive from the LiOH formed upon Li^+/H^+ exchange with residual water that remains in the pores of the washed CAM after filtration. Finally, the formation of sodium surface species was observed by XPS upon heating of as-received, wet-stored, or washed NCM851005 to 450 °C, which is ascribed to the temperature induced surface segregation of sodium sulfate that has remained from the synthesis.

Acknowledgments

Financial support by the BASF SE through its Research Network on Electrochemistry and Batteries is gratefully acknowledged.

Appendix

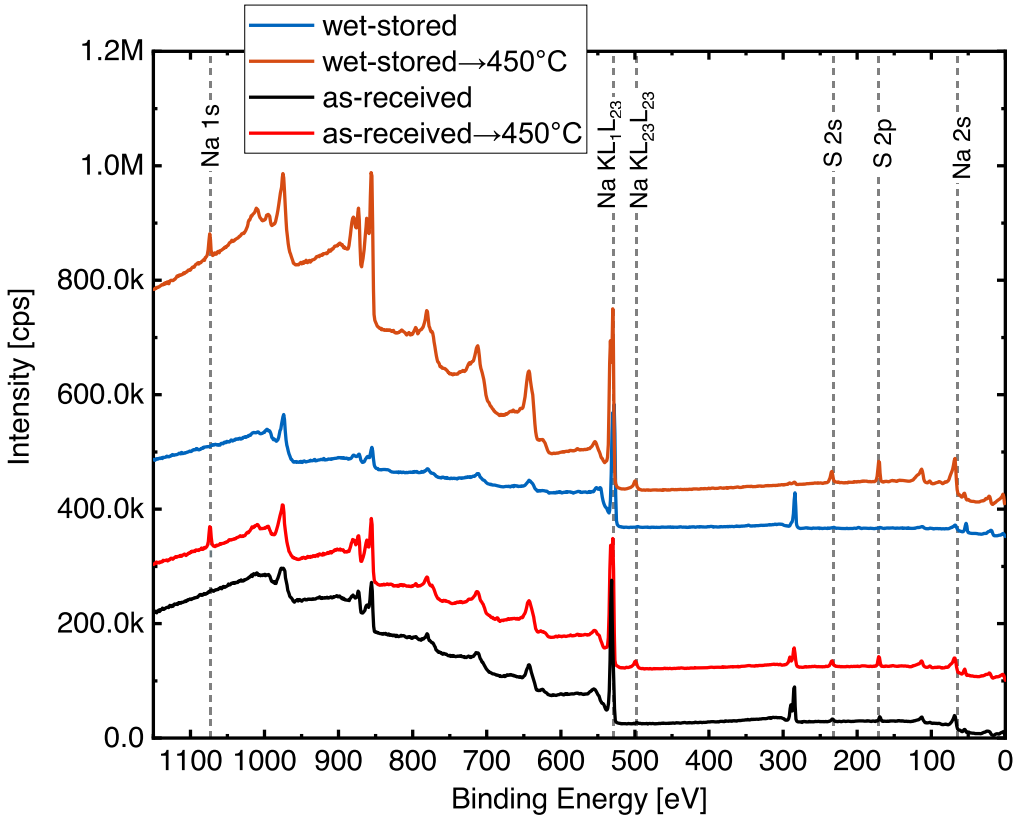

Figure A·1. XPS survey scan of the as-received NCM851005 (in black), the 1 week wet-stored NCM851005 (in blue) as well as after a 3 h heat-treatment in the XPS chamber at 450 °C (as-received in red; wet-stored in orange). The spectra were acquired with a stepsize of 0.5 eV and at a pass energy of 160 eV, using a monochromatized Al Kα source; the *y*-axis values of the spectra are offset by arbitrary constant values for better legibility of the spectra. The Na 1s and Na 2s binding energies as well as the Na KLL Auger lines are marked by vertical dashed lines; here it should be noted that for NCM materials the Co 3p and the Na 2 s features overlap, so that a peak in the Na 2s region for NCMs is not necessarily indicative of the presence of sodium. Further marked are the S 2s and S 2p binding energies.

ORCID

Louis Hartmann https://orcid.org/0000-0002-3964-1935
Hubert A. Gasteiger https://orcid.org/0000-0001-8199-8703

References

1. P. K. Nayak, E. M. Erickson, F. Schipper, T. R. Penki, N. Munichandraiah, P. Adelhelm, H. Sclar, F. Amalraj, B. Markovsky, and D. Aurbach, *Adv. Energy Mater.*, **8**, 1702397 (2018).
2. P. Rozier and J. M. Tarascon, *J. Electrochem. Soc.*, **162**, A2490 (2015).
3. D. Andre, S.-J. Kim, P. Lamp, S. F. Lux, F. Maglia, O. Paschos, and B. Stiaszny, *J. Mater. Chem. A*, **3**, 6709 (2015).
4. W. Li, H. Y. Asl, Q. Xie, and A. Manthiram, *J. Am. Chem. Soc.*, **141**, 5097 (2019).
5. A. Manthiram, *Nat. Commun.*, **11**, 1 (2020).
6. G. Girishkumar, B. Mccloskey, A. C. Luntz, S. Swanson, and W. Wilcke, *J. Phys. Chem. Lett.*, **1**, 2193 (2010).
7. B. D. Mccloskey, R. Scheffler, A. Speidel, G. Girishkumar, and A. C. Luntz, *The Journal of Physical Chemistry C*, **116**, 23897 (2012).
8. K. Zhu, C. Wang, Z. Chi, F. Ke, Y. Yang, A. Wang, W. Wang, and L. Miao, *Front. Energy Res.*, **7**, 1 (2019).
9. J. Kim, H. Ma, H. Cha, H. Lee, J. Sung, M. Seo, P. Oh, M. Park, and J. Cho, *Advanced Energy Materials*, **8**, 1702028 (2018).
10. H. H. Ryu, N. Y. Park, J. H. Seo, Y. S. Yu, M. Sharma, R. Mücke, P. Kaghazchi, C. S. Yoon, and Y. K. Sun, *Mater. Today*, **36**, 73 (2020).
11. N. Voronina, Y.-K. Sun, and S.-T. Myung, *ACS Energy Lett.*, **5**, 1814 (2020).
12. H. Ryu, N. Park, D. R. Yoon, U. Kim, C. S. Yoon, and Y. Sun, *Adv. Energy Mater.*, 2000495 (2020).
13. A. Aishova, G. Park, C. S. Yoon, and Y. Sun, *Adv. Energy Mater.*, **10**, 1903179 (2020).
14. H. Li, A. Liu, N. Zhang, Y. Wang, S. Yin, H. Wu, and J. R. Dahn, *Chem. Mater.*, **17**, 7574 (2019).
15. H. Li, M. Cormier, N. Zhang, J. Inglis, J. Li, and J. R. Dahn, *J. Electrochem. Soc.*, **166**, A429 (2019).
16. M. Bianchini, M. Roca-Ayats, P. Hartmann, T. Brezesinski, and J. Janek, *Angew. Chemie - Int. Ed.*, **58**, 10434 (2019).
17. U. H. Kim, L. Y. Kuo, P. Kaghazchi, C. S. Yoon, and Y. K. Sun, *ACS Energy Lett.*, **4**, 576 (2019).
18. H. Li, N. Zhang, J. Li, and J. R. Dahn, *J. Electrochem. Soc.*, **165**, A2985 (2018).
19. S. Yamada, M. Fujiwara, and M. Kanda, *J. Power Sources,*, **54**, 209 (1995).
20. A. Audemer, M. R. Palacin, D. Larcher, N. Sac-Epee, G. G. Amatucci, and J.-M. Tarascon, *Journal of electrochemical Society*, **144**, 4226 (1997).
21. C. Pouillerie, L. Croguennec, P. Biensan, P. Willmann, and C. Delmas, *J. Electrochem. Soc.*, **147**, 2061 (2000).
22. A. Rougier, P. Gravereau, and C. Delmas, *J. Electrochem. Soc.*, **143**, 1168 (1996).
23. T. Ohzuku, A. Ueda, and M. Nagayama, *J. Electrochem. Soc.*, **140**, 1862 (1993).
24. J. Sicklinger, M. Metzger, H. Beyer, D. Pritzl, and H. A. Gasteiger, *J. Electrochem. Soc.*, **166**, A2322 (2019).
25. R. Jung, R. Morasch, P. Karayaylali, K. Phillips, F. Maglia, C. Stinner, Y. Shao-Horn, and H. A. Gasteiger, *J. Electrochem. Soc.*, **165**, A132 (2018).
26. I. A. Shkrob, J. A. Gilbert, P. J. Phillips, R. Klie, R. T. Haasch, J. Bareño, and D. P. Abraham, *J. Electrochem. Soc.*, **164**, A1489 (2017).
27. S. M. Bak, E. Hu, Y. Zhou, X. Yu, S. D. Senanayake, S. J. Cho, K. B. Kim, K. Y. Chung, X. Q. Yang, and K. W. Nam, *ACS Appl. Mater. Interfaces*, **6**, 22594 (2014).
28. G. V. Zhuang, G. Chen, J. Shim, X. Song, P. N. Ross, and T. J. Richardson, *J. Power Sources,*, **134**, 293 (2004).
29. J. Paulsen and J. H. Kim, 2014/0054495 A1 (2014).
30. P. Paulsen and J. H. Kim, WO 2012/107313 A1 (2012).
31. D.-H. Cho, C.-H. Jo, W. Cho, Y.-J. Kim, H. Yashiro, Y.-K. Sun, and S.-T. Myung, *J. Electrochem. Soc.*, **161**, A920 (2014).
32. J. Kim, Y. Hong, K. S. Ryu, M. G. Kim, and J. Cho, *Electrochem. Solid-State Lett.*, **9**, A19 (2006).
33. A. T. S. Freiberg, J. Sicklinger, S. Solchenbach, and H. A. Gasteiger, *Electrochim. Acta*, **346**, 136271 (2020).
34. S. E. Renfrew, L. A. Kaufman, and B. D. McCloskey, *ACS Appl. Mater. Interfaces*, **11**, 34913 (2019).
35. C. Lv, Z. Li, X. Ren, K. Li, J. Ma, and X. Duan, *J. Mater. Chem. A*, **9**, 3995 (2021).
36. F. Schipper, H. Bouzaglo, M. Dixit, E. Erickson, T. Weigel, M. Talianker, J. Grinblat, L. Burstein, M. Schmidt, P. Lampert, C. Erk, B. Markovsky, D. Major, and D. Aurbach, *Adv. Energy Mater.*, **8**, 1701682 (2018).
37. L. Li, Q. Yao, H. Zhu, Z. Chen, L. Song, and J. Duan, *J. Alloys Compd.*, **686**, 30 (2016).
38. X. Liu, P. He, H. Li, M. Ishida, and H. Zhou, *J. Alloys Compd.*, **552**, 76 (2013).
39. F. A. Susai, H. Sclar, S. Maiti, L. Burstein, O. Perkal, J. Grinblat, M. Talianker, S. Ruthstein, C. Erk, P. Hartmann, B. Markovsky, and D. Aurbach, *ACS Appl. Energy Mater.*, **3**, 3609 (2020).
40. U. Breddemann et al., *ChemElectroChem*, **6**, 3337 (2019).
41. T. Shinpuku, T. Hiroshi, R. Otterstedt, and K. Keiichiro, WO 2018/172272 Al (2018).
42. J. Kim, H. Lee, H. Cha, M. Yoon, M. Park, and J. Cho, *Adv. Energy Mater.*, **8**, 1870023 (2018).
43. D. Pritzl, T. Teufl, A. T. S. Freiberg, B. Strehle, J. Sicklinger, H. Sommer, P. Hartmann, and H. A. Gasteiger, *J. Electrochem. Soc.*, **166**, A4056 (2019).
44. J. Kim, Y. Hong, K. S. Ryu, M. G. Kim, and J. Cho, *Electrochem. Solid-State Lett.*, **9**A19 (2006).
45. F. Friedrich, B. Strehle, A. T. S. Freiberg, K. Kleiner, S. J. Day, C. Erk, M. Piana, and H. A. Gasteiger, *J. Electrochem. Soc.*, **166**, A3760 (2019).
46. S. E. Renfrew and B. D. McCloskey, *J. Am. Chem. Soc.*, **139**, 17853 (2017).
47. H. Beyer, S. Meini, N. Tsiouvaras, M. Piana, and H. A. Gasteiger, *Phys. Chem. Chem. Phys.*, **15**, 11025 (2013).
48. M. Grágeda, A. González, W. Alavia, and S. Ushak, *Energy*, **89**, 667 (2015).
49. N. V. Faenza, L. Bruce, Z. W. Lebens-Higgins, I. Plitz, N. Pereira, L. F. J. Piper, and G. G. Amatucci, *J. Electrochem. Soc.*, **164**, A3727 (2017).
50. R. Jung, M. Metzger, F. Maglia, C. Stinner, and H. A. Gasteiger, *J. Phys. Chem. Lett.*, **8**, 4820 (2017).
51. S. Ahmed, A. Pokle, S. Schweidler, A. Beyer, M. Bianchini, F. Walther, A. Mazilkin, P. Hartmann, T. Brezesinski, J. Janek, and K. Volz, *ACS Nano*, **13**, 10694 (2019).
52. H. Sclar, J. Sicklinger, E. Erickson, S. Maiti, J. Grinblat, M. Talianker, F. Susai, L. Burstein, H. Beyer, L. Hartmann, G. Avruschenko, H. Gasteiger, B. Markovsky, and D. Aurbach, *J. Electrochem. Soc.*, **167**, 110563 (2020).
53. J. Sicklinger, H. Beyer, L. Hartmann, F. Riewald, C. Sedlmeier, and H. A. Gasteiger, *J. Electrochem. Soc.*, **167**, 130507 (2020).
54. M. Otoyama, Q. Jacquet, A. Iadecola, M. Saubanère, G. Rousse, and J.-M. Tarascon, *Adv. Energy Mater.*, **9**, 1803674 (2019).
55. Z. W. Lebens-Higgins et al., *J. Phys. Chem. Lett.*, **11**, 2106 (2020).
56. M. C. Biesinger, B. P. Payne, A. P. Grosvenor, L. W. M. Lau, A. R. Gerson, and R. S. C. Smart, *Appl. Surf. Sci.*, **257**, 2717 (2011).
57. A. J. Nelson, J. G. Reynolds, and J. W. Roos, *J. Vac. Sci. Technol. A Vacuum, Surfaces, Film.*, **18**, 1072 (2000).
58. F. Friedrich, B. Strehle, and H. A. Gasteiger, *ECS Meet. Abstr.*, **MA2020-02**, 254 (2020).
59. M. P. Seah and W. A. Dench, *Surf. Interface Anal.*, **1**, 2 (1979).
60. H.-J. J. Noh, S. Youn, C. S. Yoon, and Y.-K. K. Sun, *J. Power Sources,*, **233**, 121 (2013).
61. I. Hamam, N. Zhang, A. Liu, M. B. Johnson, and J. R. Dahn, *J. Electrochem. Soc.*, **167**, 130521 (2020).